Ceramics International 47 (2021) 23518–23527

Contents lists available at ScienceDirect

Ceramics International

journal homepage: www.elsevier.com/locate/ceramint

Characterization of the full matrix constants of $Bi_4Ti_3O_{12}$ ceramics

Wei Wang [b,1], Kang Zheng [b,1], Shanshan Sun [b], Lei Qin [a,*], Liguo Tang [b,c,**], Zhenglin Li [c]

[a] Beijing Key Laboratory for Sensors, Beijing Information Science & Technology University, Beijing, 100192, China
[b] Key Laboratory of Underwater Acoustic Communication and Marine Information Technology, Ministry of Education, College of Ocean and Earth Sciences, Xiamen University, Xiamen, 361010, China
[c] State Key Laboratory of Acoustics, Institute of Acoustics, Chinese Academy of Sciences, Beijing, 100190, China

ARTICLE INFO

Keywords:
BIT ceramics
Characterization
Resonant ultrasound spectroscopy
Elastic constants
Piezoelectricity

ABSTRACT

Fabricating high-quality, large-size $Bi_4Ti_3O_{12}$ (BIT) ceramics is challenging; therefore, the full matrix constants of BIT ceramics have not been characterized, which notably hinders their applications. In this study, the elastic stiffness constants c_{11}^E and c_{33}^D of the BIT ceramics were determined using the ultrasonic pulse-echo method. In addition, the elastic stiffness constants c_{12}^E, c_{13}^E, c_{33}^E, and c_{44}^E were determined using resonant ultrasound spectroscopy. Furthermore, the piezoelectric stress constants e_{15}, e_{31}, and e_{33} of BIT ceramics were calculated using the formula for the relationship between different material constants.

1. Introduction

Lead-based piezoelectric ceramics, such as lead zirconate titanate (PZT), are widely used in actuators, sensors, and transducers because of their excellent piezoelectricity [1,2]. However, harmful substances are produced during the manufacture, use, and disposal of such devices. Thus, there is a recognized need for the development of environmentally friendly lead-free materials [3–5]. Lead-free piezoelectric materials can be described as perovskites, such as $BaTiO_3$, $KNbO_3$, and $NaTaO_3$, or non-perovskites, for example, bismuth layer-structured ferroelectrics (BLSFs) and tungsten-bronze-type ferroelectrics [6]. Bismuth titanate ($Bi_4Ti_3O_{12}$; BIT) is one of the most interesting BLSF compounds [7]. It exhibits a high Curie temperature (675 °C), low dielectric constant (127–154), high mechanical quality factor (5,900), and low aging rate. As a result, it has the potential to be used in piezoelectric devices employed in the aeronautic, aerospace, and automotive industries, and should work at high temperatures, as demonstrated in previous studies. For instance, Daichi et al. [8] fabricated $LiNbO_3$/BIT ultrasonic transducers with sufficient thermal durability at 700 °C, while Xie et al. [9] enhanced the piezoelectric properties and temperature stability of BIT-based Aurivillius ceramics via W/Nb substitution. Xu et al. [10] fabricated ultrasonic transducers for high-temperature applications using BIT and Ceramabind 830, and Megriche et al. [11] prepared BIT ceramics that showed good stability up to 500 °C.

Generally, the elastic, dielectric, and piezoelectric constants of BIT should be determined before they are used to design piezoelectric devices. If these constants are known, researchers can execute numerical simulations to evaluate the properties of piezoelectric devices. Kitanaka et al. [12] determined the elastic compliance constants (s_{11}^E, s_{22}^E, s_{33}^E, and s_{66}^E), piezoelectric constants (d_{11}, d_{12}, d_{13}, and d_{26}), and coupling factors (k_{11}, k_{12}, k_{13}, and k_{26}) of BIT single crystals using the electric resonance method. In addition, Shulman et al. [13] studied the microstructure, electrical conductivity, and piezoelectric properties of BIT, while Kozielski et al. [14] studied the dielectric relaxation of BIT ceramics prepared via low-temperature combustion synthesis. Nagata et al. studied the high-temperature piezoelectric constant d_{33} and coupling factor k_{33} of vanadium-doped BIT ceramics with grain orientation [15], as well as the temperature dependence of the piezoelectric constant k_{33} and elastic compliance constant s_{33}^E on Nd and V co-substituted BIT ceramics [16]. Villegas et al. [17] determined the temperature dependence of the piezoelectric parameters k_p and d_{31} of W-doped BIT from the resonance and anti-resonance frequencies.

However, the full matrix constants, including the elastic, piezoelectric, and dielectric constants, of BIT ceramics and single crystals have not been characterized for several reasons. First, grown BIT single crystals are always in the form of very thin platelets, which makes it

* Corresponding author.
** Corresponding author. Key Laboratory of Underwater Acoustic Communication and Marine Information Technology, Ministry of Education, College of Ocean and Earth Sciences, Xiamen University, Xiamen, 361010, China..
E-mail addresses: qinlei@bistu.edu.cn (L. Qin), liguotang@xmu.edu.cn (L. Tang).
[1] These authors contributed equally to this work.

https://doi.org/10.1016/j.ceramint.2021.05.068
Received 14 March 2021; Received in revised form 9 May 2021; Accepted 10 May 2021
Available online 19 May 2021

difficult to characterize their full matrix constants [18]. Second, BIT single crystals have a monoclinic symmetry [7,19–21]. There are 13 independent elastic constants, 10 independent piezoelectric constants, and 4 independent dielectric constants. Characterization of such a large number of material constants is difficult. Moreover, BIT ceramics have low electrical resistivity and a large coercive field, which hinders the poling process. Thus, doping with one or more elements is often used to enhance the piezoelectric and ferroelectric properties of BIT-based materials. For example, doping BIT ceramics with donor cations, such as Nb (V) and W(VI), reduces the conductivity by at least one order of magnitude [7,22,23]. However, doping forms a more sophisticated structure; therefore, maintaining the uniformity of BIT ceramics during preparation is challenging. More specifically, it is difficult to ensure that prepared large BIT samples still have good uniformity. For example, the poled BIT products of the Fuji Ceramics Corporation have a thickness of only 2 mm.

The ultrasonic pulse-echo (UPE) method and the IEEE impedance resonant method are commonly used to characterize the full matrix constants of piezoelectric materials [24]. The UPE method can be used to determine some elastic constants instead of all elastic constants of an anisotropic sample. The impedance resonant method requires multiple samples with drastically different geometric sizes during the characterization. The small size of a BIT sample limits the use of this method in its characterization. The k_{15} resonator can be used as an example to illustrate this problem. The dimensions of the k_{15} resonator assumed along the *x*-, *y*-, and *z*-directions are *t*, *w*, and *l*, respectively, where *z* is the polarization direction. Theoretically, to ensure the accuracy of the characterization, *l* and *w* should be considerably greater than *t*. In practical measurements, it is generally required that both *l*/*t* and *w*/*t* exceed 10. If *l* is 2 mm, then *t* should be less than 0.2 mm. When such a thin sample is clamped by a fixer connected to an impedance analyzer, a large measurement error may occur. In addition, the full matrix constants characterized using the impedance resonant method are probably inconsistent because multiple samples are used in the characterization [25–27].

In this study, the resonant ultrasound spectroscopy (RUS) technique was used to determine the elastic constants of BIT samples. RUS is suitable for characterizing BIT for the following two reasons. First, it can characterize the material constants of samples with very small sizes (<1 mm^3) [28–30]. Second, this technique can be used to characterize a sample with a high mechanical quality factor (Q_M), while that of BIT is approximately 5900. As early as 1990, Ohno [31] first utilized RUS to retrieve the elastic constants of piezoelectric materials. Ogi and his colleagues [32–34] characterized the full matrix constants of lithium niobate, α-quartz, and GaN, all of which have a very high Q_M. In another study, Tang et al. [27] determined the temperature dependence of the full matrix constants of PZT-4 via RUS, while Chen et al. [35] employed RUS to characterize the elastic and piezoelectric constants of single-domain 0.72 $Pb(Mg_{1/3}Nb_{2/3})O_3$–0.28$PbTiO_3$ single crystals. Finally, Xiang et al. [36] characterized the elastic and piezoelectric properties of a single-domain $Pb(Zn_{1/3}Nb_{2/3})O_3$–6.5%$PbTiO_3$ single crystal using RUS.

The combination of UPE and RUS employs only one piezoelectric sample to characterize all the elastic constants of a BIT ceramic sample. The dielectric constants were measured directly using an impedance analyzer from the same sample. The piezoelectric stress constants e_{31} and e_{33} can be calculated using the formula for the relationship between different material constants. The value of e_{15} was assumed to be approximately zero according to the RUS inversion results. Therefore, all constants were determined from the same sample to ensure consistency of the results.

2. Methodology

2.1. Principle of resonant ultrasound spectroscopy (RUS)

RUS contains two problems: forward and inverse. The RUS forward problem uses the Rayleigh–Ritz method to calculate resonance frequencies based on the material constants and geometric dimensions of a sample. The RUS inverse problem uses the least-squares method to inverse material constants based on the measured resonance frequencies of a sample.

2.1.1. Forward problem

The Lagrangian for electroelastic vibrations is given by

$$L=\frac{1}{2}\int_V\left(S_{ij}c^E_{ijkl}S_{kl}-\phi_{,m}\varepsilon^S_{mn}\phi_{,n}+2\phi_{,m}e_{mkl}S_{kl}-\rho\omega^2u_iu_i\right)dV, \tag{1}$$

where S_{ij} is the strain tensor, $c^{\mathrm{E}}_{\mathrm{ijkl}}$ is the elastic stiffness tensor at a constant electric field, ϕ is the elastic potential, $\varepsilon^{\mathrm{S}}_{\mathrm{mn}}$ is the dielectric tensor at constant mechanical strain, e_{mlk} is the piezoelectric tensor, ρ is the density, ω is the angular frequency, and u_i is the displacement. The electric potential ϕ and displacement u_i can be expressed as

$$\phi=\sum_{r=1}^{M}b_r\psi_r, \tag{2}$$

and

$$u_i=\sum_{p=1}^{N}a_p^{(i)}v_p, \tag{3}$$

where $\{\psi_r\}$ and $\{v_p\}$ are orthogonal basis functions, and b_r and $a_p^{(i)}$ are the corresponding expansion coefficients. Let *L* take the derivation of b_r and $a_p^{(i)}$ and set them to zero.

$$\frac{\partial L}{\partial b_r}=0, r=1,2,3\ldots,M \tag{4a}$$

$$\frac{\partial L}{\partial a_p^{(i)}}=0, p=1,2,3\ldots,N \tag{4b}$$

Substituting Eqs. (4a) and (4b) into Eq. (1), we have

$$\left(\mathbf{\Gamma}+\mathbf{\Omega}\mathbf{\Lambda}^{-1}\mathbf{\Omega}^{T}\right)\mathbf{A}=\left(p\omega^2\right)\mathbf{A} \tag{5}$$

and

$$\mathbf{B}=\mathbf{A}^{-1}\mathbf{\Omega}^{\mathrm{T}}\mathbf{A}, \tag{6}$$

where

$$\mathbf{A}=\left[a_1^{(1)},a_2^{(1)},\ldots,a_N^{(1)},a_1^{(2)},a_2^{(2)},\ldots,a_N^{(2)},a_1^{(3)},a_2^{(3)},\ldots,a_N^{(3)}\right], \tag{7}$$

$$\mathbf{B}=[b_1,b_2,\cdots,b_M], \tag{8}$$

and $\mathbf{\Gamma}$, $\mathbf{\Omega}$, and $\mathbf{\Lambda}$ are the elastic, piezoelectric, and dielectric matrices, respectively. The elements of $\mathbf{\Gamma}$, $\mathbf{\Omega}$, and $\mathbf{\Lambda}$ can be expressed as

$$\Gamma^{ik}_{pp'}=\iiint v_{p,j}c_{ijkl}v_{p',l}dV, (i,k=1,2,3), \tag{9}$$

$$\Omega^{k}_{rp}=\iiint \psi_{r,m}e_{mkl}v_{p,l}dV, (k=1,2,3), \tag{10}$$

and

$$\Lambda_{rr'}=\iiint \psi_{r,m}\varepsilon_{mn}\psi_{r',n}dV, \tag{11}$$

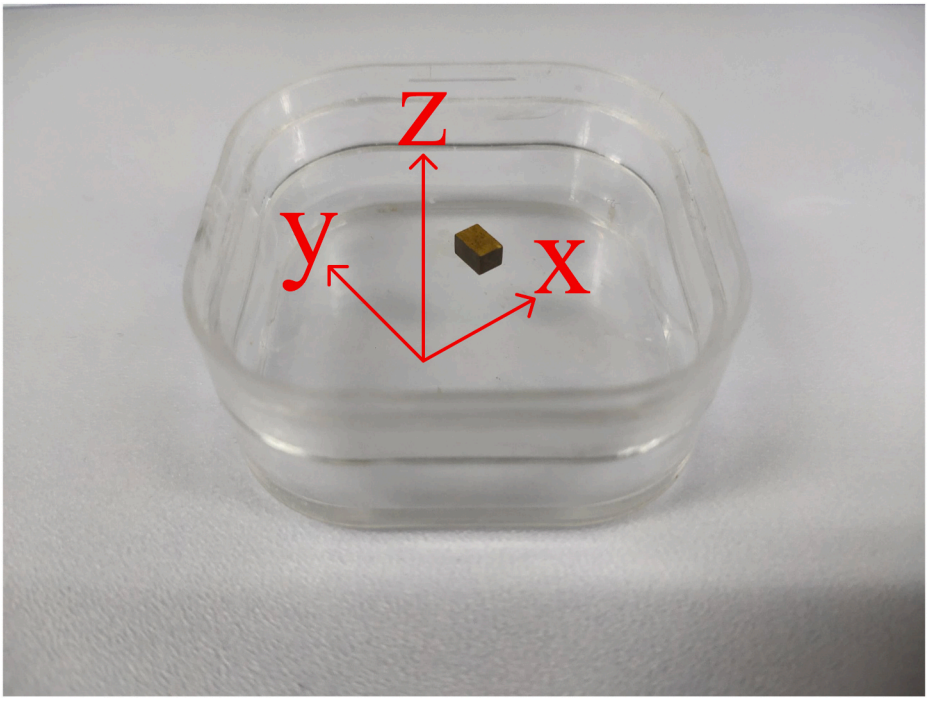

Fig. 1. Bismuth titanate (BIT) ceramic sample.

respectively. The resonance frequencies can be obtained by solving the eigenvalue problem given in Eq. (5).

2.1.2. Inverse problem

The use of measured resonant frequencies to determine the material constants of a sample is essentially a nonlinear least-squares problem of finding the local minimizer of the following equation:

$$F = \frac{1}{2}\sum_{i=1}^{K} w_i \left[f_{cal}^{(i)} - f_{meas}^{(i)}\right]^2, \tag{12}$$

where w_i is the weighting factor, and $f_{\mathrm{meas}}^{(\mathrm{i})}$ and $f_{\mathrm{cal}}^{(\mathrm{i})}$ are the i^{th} measured and calculated resonance frequencies, respectively. The Levenberg–Marquardt (LM) algorithm is often used to solve this problem [37]. In this algorithm, the iteration step is calculated as

$$\left(\mathbf{J}^{\mathrm{T}}\mathbf{J} + \mu\mathbf{I}\right)h_{\mathrm{LM}} = -\mathbf{J}^{\mathrm{T}}\mathbf{f}, \tag{13}$$

where **J** is the Jacobi matrix, **I** is the identity matrix, μ is the damping parameter, T is the matrix transpose, h_{LM} is the step size, and **f** is the vector of the difference between the calculated and measured resonance frequencies. The elements of **f** can be expressed as

$$f^{(i)} = f_{cal}^{(i)} - f_{meas}^{(i)}. \tag{14}$$

2.2. Experimental procedure

In this study, the BIT ceramic was seen as a 6mm point group structure. Therefore, the matrices of the elastic constant $\mathbf{c}^{\mathrm{E}}$, piezoelectric constant **e**, and dielectric constant $\boldsymbol{\varepsilon}^{\mathrm{S}}$ can be formulated as

$$\mathbf{c}^{\mathrm{E}} = \begin{bmatrix} c_{11}^{\mathrm{E}} & c_{12}^{\mathrm{E}} & c_{13}^{\mathrm{E}} & 0 & 0 & 0 \\ c_{12}^{\mathrm{E}} & c_{11}^{\mathrm{E}} & c_{13}^{\mathrm{E}} & 0 & 0 & 0 \\ c_{13}^{\mathrm{E}} & c_{13}^{\mathrm{E}} & c_{33}^{\mathrm{E}} & 0 & 0 & 0 \\ 0 & 0 & 0 & c_{44}^{\mathrm{E}} & 0 & 0 \\ 0 & 0 & 0 & 0 & c_{44}^{\mathrm{E}} & 0 \\ 0 & 0 & 0 & 0 & 0 & \dfrac{c_{11}^{\mathrm{E}} - c_{12}^{\mathrm{E}}}{2} \end{bmatrix}, \tag{15}$$

$$\mathbf{e} = \begin{bmatrix} 0 & 0 & 0 & 0 & e_{15} & 0 \\ 0 & 0 & 0 & e_{15} & 0 & 0 \\ e_{31} & e_{31} & e_{33} & 0 & 0 & 0 \end{bmatrix}, \tag{16}$$

and

$$\boldsymbol{\varepsilon}^{\mathrm{S}} = \begin{bmatrix} \varepsilon_{11}^{S} & 0 & 0 \\ 0 & \varepsilon_{11}^{S} & 0 \\ 0 & 0 & \varepsilon_{33}^{S} \end{bmatrix}, \tag{17}$$

respectively. All measurements described in this section were conducted at room temperature.

2.2.1. Measurements of geometric parameter and mass

Fig. 1 shows a rectangular parallelepiped BIT ceramic sample purchased from Fuji Ceramics Corporation. The size and mass of the sample were measured using a micrometer and an analytical balance, respectively. The sample size was 2.335 mm × 3.399 mm × 1.967 mm. The density determined using Archimedes' method was 7240 kg/m^3.

2.2.2. Measurement of dielectric constants

The low-frequency capacitances at 1 kHz and high-frequency capacitances at 30 MHz of the BIT sample were measured using a Tonghui 2838H and HP 4194A impedance analyzer, respectively. The free and

Table 1
Relative dielectric constants of the BIT sample.

$\varepsilon_{11}^{T}/\varepsilon_0$	$\varepsilon_{33}^{T}/\varepsilon_0$	$\varepsilon_{11}^{S}/\varepsilon_0$	$\varepsilon_{33}^{S}/\varepsilon_0$
–	144	145	138

clamped dielectric constants were obtained from the low- and high-frequency capacitances, respectively. For example, the free and clamped dielectric constants ε_{33}^{T} and ε_{33}^{S} can be obtained using

$$\varepsilon_{33}^{T} = \frac{C_3^L t}{lw} \tag{18}$$

and

$$\varepsilon_{33}^{S} = \frac{C_3^H t}{lw}, \tag{19}$$

respectively, where C_3^L and C_3^H are the low- and high-frequency capacitances along the z-axis direction, respectively; and l, w and t are sample sizes along the x-, y-, and z-axis directions, respectively. Table 1 lists the relative dielectric constants of the BIT sample.

2.2.3. Measurement of some elastic constants

Some elastic constants of the BIT sample were determined using the UPE method. A 10-MHz longitudinal wave transducer (Olympus, CN10R-5) and a 5-MHz shear wave transducer (Olympus, V156-RM) were used to transmit and receive longitudinal and shear waves, respectively. The transducers were excited by a 30-MHz pulser/receiver (Goworld Co., Ltd.), and the time of flight between the echoes was

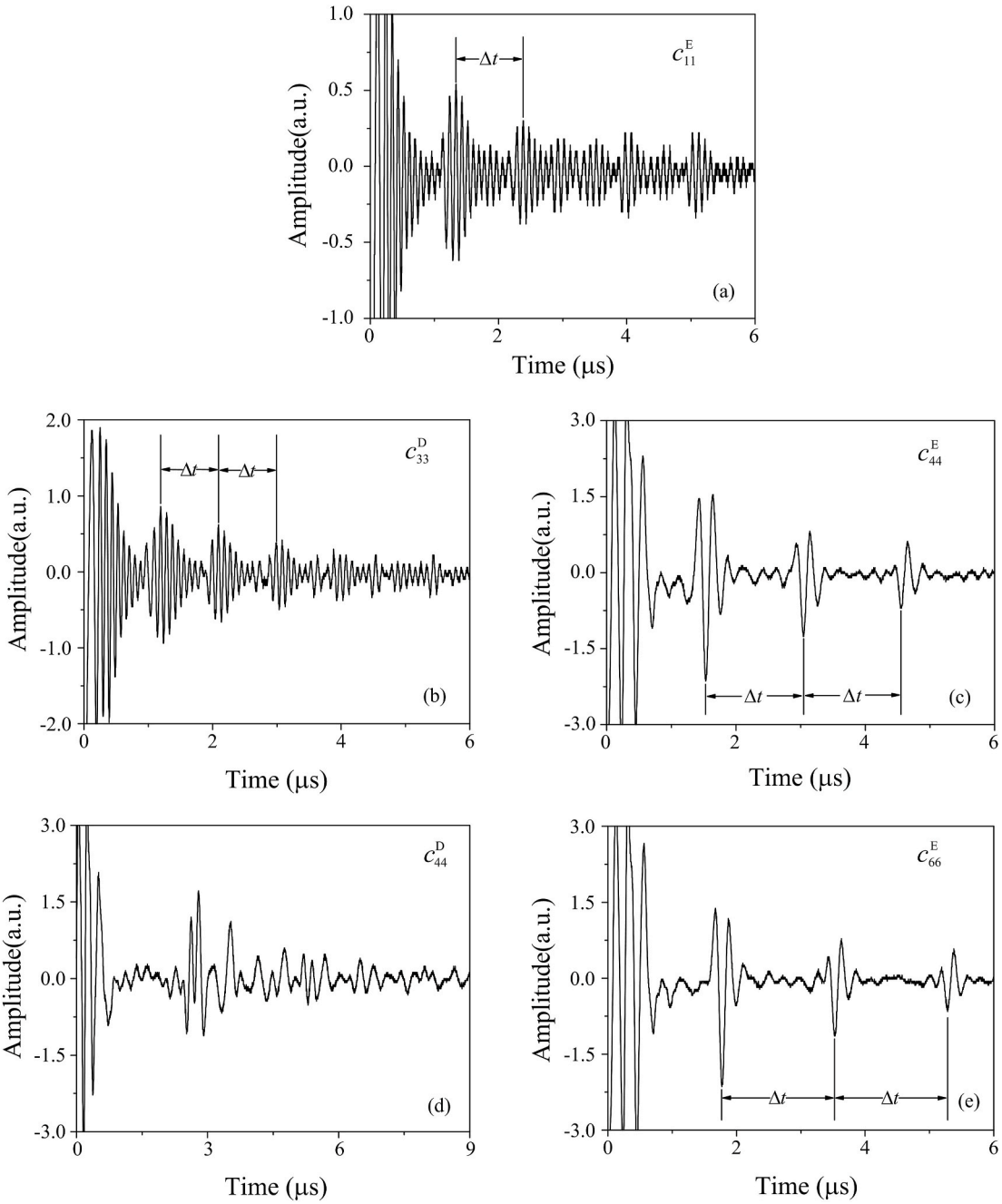

Fig. 2. Sample pulses corresponding to different elastic constants from UPE: (a) c_{11}^{E}; (b) c_{33}^{D}; (c) c_{44}^{E}; (d) c_{44}^{D}; (e) c_{66}^{E}.

Table 2
Elastic constants of BIT ceramic sample determined using the ultrasonic pulse-echo (UPE) method.

Elastic constant	c_{11}^{E}	c_{33}^{D}	c_{44}^{E}	c_{44}^{D}	c_{66}^{E}
Value (10^{10} N/m^2)	14.35	13.83	4.90	–	5.13

measured using a digital oscilloscope. The measured pulses corresponding to c_{11}^{E}, c_{33}^{D}, c_{44}^{E}, c_{44}^{D}, and c_{66}^{E} are shown in Fig. 2. The elastic constant c can be calculated using $c = \rho v^2$, where ρ and v are the density and phase velocity, respectively. Table 2 shows the elastic constants of the BIT ceramic sample determined using the UPE method. Theoretically, the values of c_{11}^{E}, c_{33}^{D}, c_{44}^{E}, c_{44}^{D}, and c_{66}^{E} can be directly measured via UPE. Unfortunately, it is difficult to determine the first two echoes in Fig. 2(d). Therefore, c_{44}^{D} cannot be precisely determined using the UPE

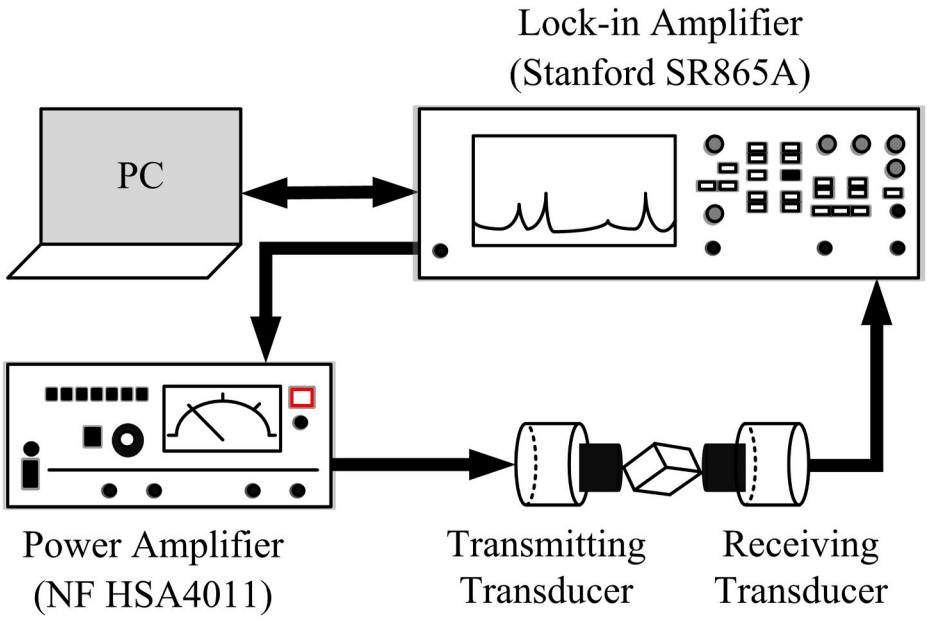

Fig. 3. Resonant ultrasound spectroscopy (RUS) experimental setup.

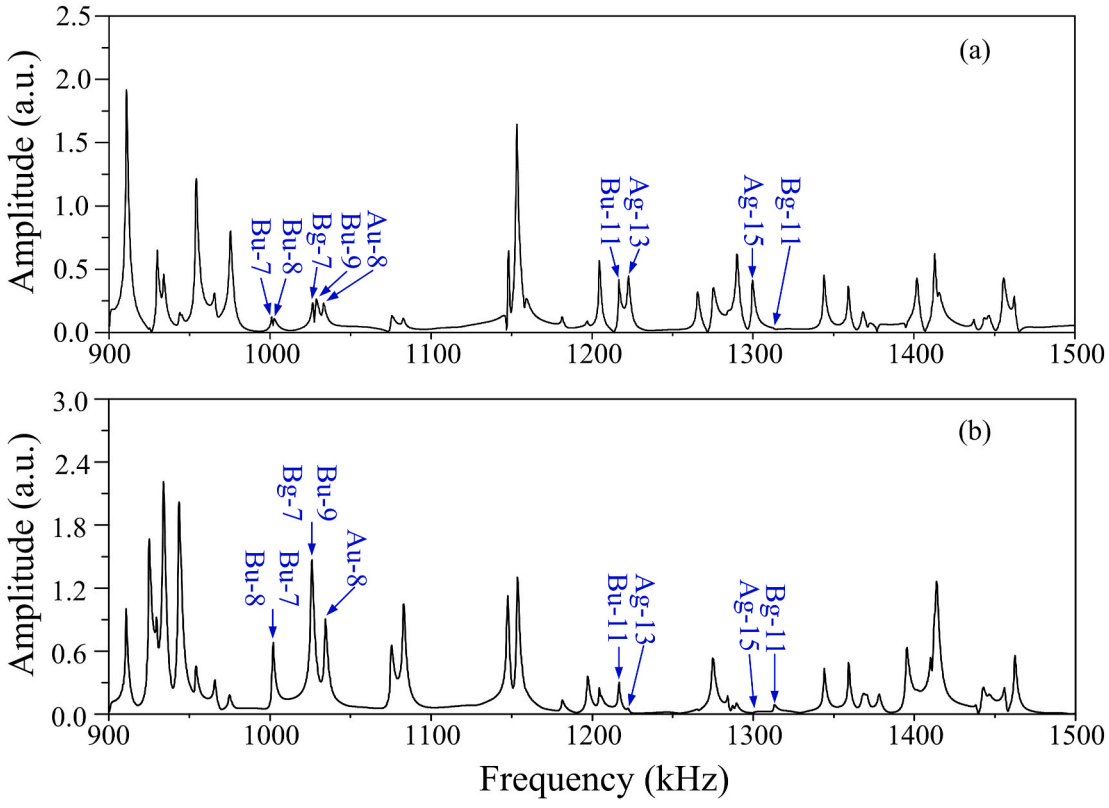

Fig. 4. Resonant ultrasonic spectra of the BIT sample from 900 to 1500 kHz.

Table 3
Measured and calculated resonance frequencies of BIT sample.

Mode	f_{meas}(kHz)	f_{cal}(kHz)	diff(%)[a]	Mode	f_{meas}(kHz)	f_{cal}(kHz)	diff(%)[a]
Au-1	348.938	346.791	0.62	Bu-10	1181.438	1183.685	0.19
Au-2	421.641	421.926	0.07	Bg-9	1196.766	1198.626	0.16
Bu-1	452.016	451.905	0.02	Ag-12	1204.219	1206.337	0.18
Ag-1	590.813	591.411	0.10	Au-11	1206.469	1206.4	0.01
Ag-2	593.484	594.184	0.12	Bu-11	1216.453	1218.46	0.16
Au-3	627.516	626.035	0.24	Ag-13	1222.359	1223.124	0.06
Bg-1	632.719	632.306	0.07	Bu-12	1265.672	1267.206	0.12
Bg-2	657.891	656.443	0.22	Bu-13	1274.531	1272.299	0.18
Au-4	709.219	708.99	0.03	Ag-14	1284.093	1284.082	0.00
Bg-3	742.547	742.474	0.01	Au-12	1287.046	1289.022	0.15
Ag-3	756.750	756.908	0.02	Bg-10	1289.719	1290.748	0.08
Bu-2	765.469	765.612	0.02	Ag-15	1299.563	1301.722	0.17
Bg-4	766.313	765.835	0.06	Bg-11	1313.203	1316.766	0.27
Bg-5	779.250	778.116	0.15	Bu-14	1344.000	1347.33	0.25
Ag-4	843.516	847.298	0.45	Bg-12	1359.188	1365.198	0.44
Bu-3	862.359	865.117	0.32	Bg-13	1368.328	1367.47	0.06
Ag-5	900.469	903.97	0.39	Au-13	1371.563	1372.485	0.07
Au-5	–	909.711	–	Bu-15	1377.609	1377.046	0.04
Bu-4	910.734	911.452	0.08	Ag-16	1395.188	1397.476	0.16
Ag-6	924.515	925.374	0.09	Bu-16	1401.797	1400.907	0.06
Bu-5	929.859	932.313	0.26	Bu-17	1409.531	1411.411	0.13
Au-6	933.656	933.165	0.05	Au-14	1412.625	1412.752	0.01
Bu-6	943.359	943.989	0.07	Ag-17	1415.578	1414.601	0.07
Bg-6	945.328	946.976	0.17	Bg-14	1437.375	1439.397	0.14
Au-7	954.047	954.63	0.06	Ag-18	1443.141	1440.155	0.21
Ag-7	965.578	965.666	0.01	Bu-18	1445.813	1447.535	0.12
Ag-8	975.000	975.437	0.04	Au-15	1455.656	1459.205	0.24
Bu-7	1001.015	1000.489	0.05	Bg-15	1462.125	1465.632	0.24
Bu-8	1002.563	1004.696	0.21	Ag-19	1513.594	1514.912	0.09
Bg-7	1026.328	1024.115	0.22	Bg-16	1518.516	1518.838	0.02
Bu-9	1028.719	1026.833	0.18	Ag-20	1531.453	1533.135	0.11
Au-8	1033.219	1033.208	0.00	Au-16	1533.984	1536.064	0.14
Au-9	1075.687	1074.222	0.14	Bg-17	1535.813	1538.536	0.18
Ag-9	1082.859	1081.435	0.13	Au-17	1537.922	1539.703	0.12
Ag-10	1146.413	1144.412	0.17	Bu-19	1553.812	1556.29	0.16
Au-10	1147.969	1148.736	0.07	Bu-20	1572.515	1575.985	0.22
Bg-8	1153.172	1153.297	0.01	Bu-21	1591.922	1594.328	0.15
Ag-11	1158.000	1160.802	0.24	Bu-22	1596.422	1598.815	0.15

[a] $\text{diff} = \left|\frac{f_{meas} - f_{cal}}{(f_{meas} + f_{cal})/2}\right| \times 100.$

method. The value of c_{12}^E calculated using $c_{12}^E = c_{11}^E - 2\,c_{66}^E$ is 4.09×10^{10} N/m^2. Note that the values of c_{11}^E, c_{12}^E, c_{44}^E determined by UPE can be used as the initial values in the RUS inversion.

2.2.4. Measurement of resonant ultrasound spectra

Fig. 3 shows the RUS experimental setup, which comprised transmitting and receiving transducers, an NF HSA4011 power amplifier, a Stanford SR865A lock-in amplifier, and a personal computer (PC). The sample was fixed between the transmitting and receiving transducers, with contact only at the opposite corners. The lock-in amplifier produced a frequency-sweeping signal, which was the input to the power amplifier and thus amplified. The transmitting transducer was driven by an amplified signal. Consequently, the vibrations of the sample were excited. The vibration was sensed by the receiving transducer and converted into an electrical signal that was input to the lock-in amplifier. After processing, the resonance spectrum of the sample was output from the lock-in amplifier and displayed on the PC.

3. Results and discussion

3.1. Results of RUS

In RUS, the sample position significantly influences the measured resonant ultrasound spectrum. Some modes that are missed in the measured spectrum may occur in another position. To perform accurate mode identification, multiple sets of spectra from 300 to 2000 kHz were measured by changing the sample position. Two sets of ultrasonic resonance spectra of the BIT sample from 900 to 1500 kHz are shown in Fig. 4. The rectangular parallelepiped BIT ceramic sample has four vibration groups denoted by A_g, B_g, A_u, and B_u, respectively, according to the deformation symmetry [31]. Modes B_u-7 and B_u-8, as well as B_g-7 and B_u-9, overlap. They cannot be identified from Fig. 4(b); however, they can be identified from Fig. 4(a). Modes A_g-13 and A_g-15 can be precisely identified from Fig. 4(a), but they are difficult to identify from Fig. 4(b). Meanwhile, mode B_g-11 can be identified from Fig. 4(b) but not Fig. 4(a). 75 resonance modes were identified from the measured

Table 4
Inversion results of BIT sample using a different number of resonance modes.

Modes	Elastic constant c_{ij}^E (10^{10} N/m^2)					Piezoelectric constant e_{ij} (C/m^2)		
	c_{11}^E	c_{12}^E	c_{13}^E	c_{33}^D	c_{44}^E	e_{15}	e_{31}	e_{33}
65	14.35	4.173	4.243	13.51	4.899	0.209	0.828	1.881
75	14.35	4.180	4.245	13.51	4.898	0.161	0.797	1.906
Relative error	–	0.17%	0.05%	0.0%	0.02%	26%	3.8%	1.3%

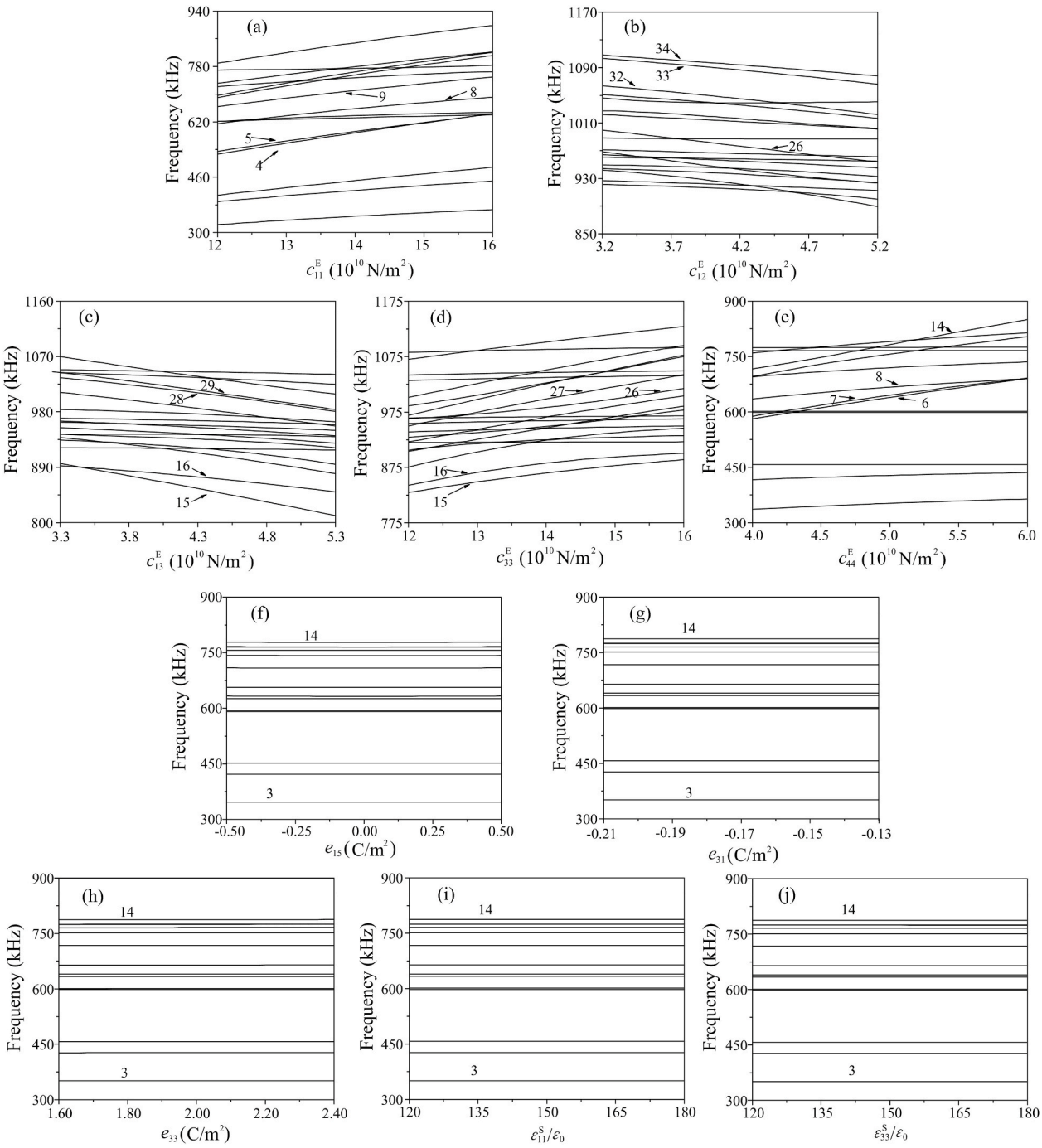

Fig. 5. Sensitivity of the resonance frequency to different material constants: (a) c_{11}^{E}; (b) c_{12}^{E}; (c) c_{13}^{E}; (d) c_{33}^{E}; (e) c_{44}^{E}; (f) e_{15}; (g) e_{31}; (h) e_{33}; (i) ε_{11}^{S}; (j) ε_{33}^{S}.

spectra, as shown in Table 3.

3.2. Inversion results

Table 4 shows the inversion results of the elastic stiffness constants c_{12}^{E}, c_{13}^{E}, c_{33}^{E} and c_{44}^{E} at a constant electric field and the piezoelectric stress constants e_{15}, e_{31} and e_{33}. Note that the value of c_{11}^{E} in Table 4 was determined by UPE. The results were obtained using 65 and 75 resonance modes. Table 4 suggests that the elastic constants are stable. The relative errors corresponding to all elastic constants were less than 0.17%. Moreover, the inversion result of c_{44}^{E} agrees very well with that determined using UPE, as shown in Table 2. The relative errors corresponding to e_{15} and e_{31} are 26% and 3.8%, respectively, which means that their inversions are unstable.

For piezoelectric materials, there are too many independent constants. It is very difficult to analyze the influence of multiple variables on resonance modes. Fig. 5 shows the sensitivity of the resonance frequencies to different material constants. The dimensions and density used in the computation were the same as those described in Section 2.2.1. The clamped dielectric constants are presented in Table 1. The elastic constants were determined from the 75 modes, as shown in Table 4. The piezoelectric constants are as follows: e_{15} = 0 C/m^2, e_{31} = -0.17 C/m^2 and e_{33} = 2.0 C/m^2. To investigate the influence of each material constant on the different modes, the resonance frequencies were computed by changing the value of a particular constant with other fixed constants. Fig. 5(a)–5(e) show that many modes are sensitive to

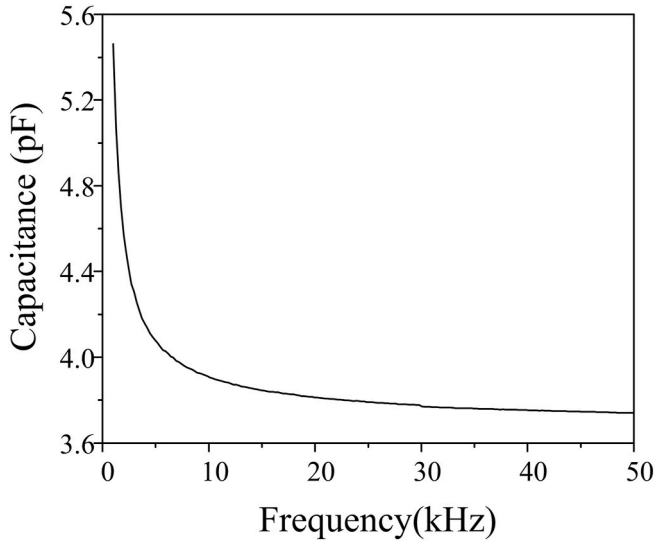

Fig. 6. Capacitance of the BIT sample along the *x*-axis from 1 to 50 kHz.

elastic constants c_{11}^E, c_{12}^E, c_{13}^E, c_{33}^E, and c_{44}^E. For example, modes 4, 5, 8, and 9 are sensitive to *c*E 11; modes 16 and 32–34 are sensitive to *c*E 12; modes 15, 16, 28, and 29 are sensitive to *c*E 13; modes 15, 16, 26, and 27 are very sensitive to *c*E 33; and modes 6–8 and 14 are very sensitive to *c*E 44. Generally, the constant can be determined by RUS if there are sufficient modes sensitive to it. However, Landa et al. [38] reported that the resonant frequencies of the single-crystal CuAlNi sample have a strong correlation with $c_{11} - c_{12}$, while they have a weak correlation with $c_{11} + c_{12}$. Hurley et al. [39] obtained the same result for textured copper. This means that small experimental errors in frequency measurements can induce large deviations in the inversion results of c_{11} and c_{12}, whereas the value of $c_{11} - c_{12}$ may not change significantly [40]. One way to overcome this problem is to determine the value of c_{11} using UPE instead of RUS [41]. Another method is to change the geometry of the sample [40]. In this study, the value of c_{11}^E was determined using UPE, as shown in Table 2..

Fig. 5(f)–5(j) show that most modes are very insensitive to the piezoelectric constants e_{15}, e_{31}, and e_{33}, and the clamped dielectric constants ε_{11}^S and ε_{33}^S. Table 4 shows that the inversion results corresponding to e_{15} and e_{31} are unstable. However, the clamped dielectric constants ε_{11}^S and ε_{33}^S can be directly determined using an impedance analyzer.

3.3. Determination of e_{15}, e_{31}, and e_{33}

Although e_{33} cannot be precisely determined via RUS, it can be determined using the following equation:

$$e_{33} = \sqrt{\varepsilon_{33}^S (c_{33}^D - c_{33}^E)} \tag{20}$$

because ε_{33}^S can be precisely determined using an impedance analyzer, as shown in Table 1, and c_{33}^D and c_{33}^E can be precisely determined via UPE and RUS, respectively. The values of c_{33}^D and c_{33}^E are shown in Tables 2 and 4, respectively. The value of e_{33}, determined using Eq. (20), is 1.98 C/m^2.

The piezoelectric stress constant e_{31} can be determined using

$$e_{31} = \frac{d_{33} - e_{33} s_{33}^E}{2 s_{13}^E}, \tag{21}$$

where the value of the piezoelectric strain constant d_{33} determined by a d_{33}-meter (ZJ-6A, Institute of Acoustics, Beijing, China) is 17.5 × 10^{-12} C/N, and the values of s_{13}^E and s_{33}^E computed from the inversion of the elastic stiffness matrix [c^E] are -1.981 × 10^{-12} and 8.647 × 10^{-12} m^2/N, respectively. The value of e_{31}, determined using Eq. (21), is -0.096 C/m^2.

Theoretically, e_{15} can be calculated from $e_{15} = \sqrt{\varepsilon_{11}^S (c_{44}^D - c_{44}^E)}$ or $e_{15} = \sqrt{c_{44}^E (\varepsilon_{11}^T - \varepsilon_{11}^S)}$ but c_{44}^D cannot be precisely determined using UPE, as mentioned in Section 2.2.3. In particular, the free dielectric constant should be measured under constant (zero) stress [1]. However, it is difficult to realize the constants at a constant stress. The conventional measurement at 1 kHz provided free dielectric constants. Fig. 6 shows the capacitance C_1 of the BIT sample along the *x*-axis from 1 to 50 kHz. Here, it can be observed that C_1 decreases exponentially with an increase in frequency from 1 to 20 kHz. Therefore, using C_1 at 1 kHz to determine ε_{11}^T might lead to inaccurate results in this case. More specifically, it is

Table 5
Full matrix material constants of the BIT ceramic sample.

c_{ij}^E (10^{10} N/m2)					c_{ij}^D (10^{10} N/m2)				
c_{11}^E	c_{12}^E	c_{13}^E	c_{33}^E	c_{44}^E	c_{11}^D	c_{12}^D	c_{13}^D	c_{33}^D	c_{44}^D
14.35	4.180	4.245	13.51	4.898	14.35	4.181	4.229	13.83	4.898
s_{ij}^E (10^{-12} m^2/N)					s_{ij}^D (10^{-12} m^2/N)				
s_{11}^E	s_{12}^E	s_{13}^E	s_{33}^E	s_{44}^E	s_{11}^D	s_{12}^D	s_{13}^D	s_{33}^D	s_{44}^D
8.069	-1.764	-1.981	8.647	20.42	8.052	-1.781	-1.918	8.403	20.42

e_{ij} (C/m^2)			d_{ij} (10^{-12} C/N)		
e_{15}	e_{31}	e_{33}	d_{15}	d_{31}	d_{33}
0.00	-0.096	1.98	0.00	-4.53	17.5
g_{ij} (10^{-3} Vm/N)			h_{ij} (10^8 V/m)		
g_{15}	g_{31}	g_{33}	h_{15}	h_{31}	h_{33}
0.00	-3.55	13.7	0.00	-0.786	16.2

ε_{ij}^T (ε_0)		ε_{ij}^S (ε_0)		β_{ij}^T (10^{-4}/ε_0)		β_{ij}^S (10^{-4}/ε_0)	
ε_{11}^T	ε_{33}^T	ε_{11}^S	ε_{33}^S	β_{11}^T	β_{33}^T	β_{11}^S	β_{33}^S
145	144	145	138	69.0	69.4	69.0	72.5
k_{ij}							
k_{15}	k_{31}	k_{33}	k_t				
0	0.05	0.17	0.15				

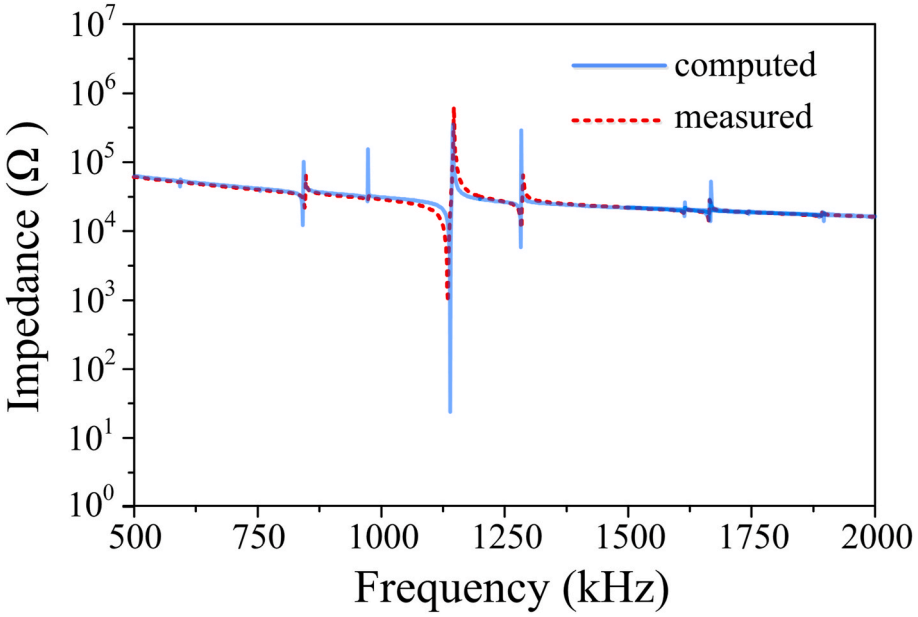

Fig. 7. Measured (red line) and computed (blue line) electrical impedance curves from 500 to 2000 kHz. (For interpretation of the references to colour in this figure legend, the reader is referred to the Web version of this article.)

difficult to precisely determine the value of e_{15} for the BIT sample using the two equations above. However, the inversion results of the RUS analysis can provide an approximate range of e_{15}. Table 4 shows that the value of e_{15} is very small. Therefore, we assume that the value of e_{15} is approximately zero.

3.4. Full matrix constants

Other material constants of BIT ceramics can be calculated using the elastic stiffness constants at a constant electric field determined via RUS using 75 resonance modes (Table 4), clamped dielectric constants (Table 1), and piezoelectric stress constants (Section 3.3). Table 5 shows the full matrix material constants of the BIT ceramic sample, including the elastic stiffness constant at constant electric field c_{ij}^{D}; elastic stiffness constant at constant electric displacement c_{ij}^{D}; elastic compliance constant at constant electric field s_{ij}^{E}; elastic compliance constant at constant electric displacement s_{ij}^{D}; piezoelectric voltage constant g_{ij}; piezoelectric stiffness constant h_{ij}; piezoelectric strain constants d_{ij}; free and clamped dielectric isolation rates β_{ij}^{T} and β_{ij}^{S}, respectively; and electromechanical coupling constants k_{ij}.

3.5. Verification of results

The values of f_{cal} in Table 3 are the resonance frequencies calculated using the elastic, piezoelectric, and dielectric constants shown in Table 5. The relative errors between the measured and calculated resonance frequencies are presented in Table 3. Most of them are less than 0.3%, which indicates that the results determined here are reliable.

Fig. 7 shows the electrical impedance curves from 500 to 2000 kHz, where the red dotted line was measured using the Tonghui 2838H impedance analyzer, and the blue line was computed using ABAQUS (Dassault Systèmes Simulia Corp., Providence, RI). During the simulation, the elastic constants were determined via RUS using 75 modes, as shown in Table 4. The clamped dielectric constants are listed in Table 1, and the piezoelectric constants are those given in Section 3.3. Complex material constants should be used to simulate the precise electrical impedance. Only real elastic, piezoelectric, and dielectric constants were used during the finite element simulation. Therefore, the amplitudes of the measured and simulated impedances are usually inconsistent. However, the resonance and anti-resonance frequencies were determined by the real material constants. Fig. 6 shows that most of the measured and simulated resonance and anti-resonance frequencies agree well. This finding verifies the reliability of the material constants of BIT determined in this study.

4. Conclusions

Multiple piezoelectric samples with drastically different sizes are required by the IEEE impedance resonant method to determine their full matrix constants. However, it is exceedingly difficult to fabricate large, high-quality poled BIT ceramics. Therefore, the full matrix constants of BIT ceramics have not yet been published. To solve this problem, in this study, RUS was introduced to characterize BIT ceramics. RUS is suitable for determining the material constants of a small sample with a high Q_M. Five independent elastic constants at a constant electric field of the BIT ceramic sample, c_{11}^{E}, c_{12}^{E}, c_{13}^{E}, c_{33}^{E}, and c_{44}^{E}, were determined via UPE and RUS using only one small sample. The clamped dielectric constants ε_{11}^{S} and ε_{33}^{S} of the BIT sample were determined from the high-frequency capacitances measured using the impedance analyzer. The elastic constant c_{33}^{D} was determined using the UPE method. Furthermore, the piezoelectric stress constants e_{31} and e_{33} of BIT were calculated using the formula for the relationship between different material constants. The value of e_{15} was assumed to be approximately zero according to the RUS inversion results. To verify the reliability of the determined results, the electric impedance spectra calculated using these results were compared with those directly measured using an impedance analyzer.

The results of this study will be helpful in the design of piezoelectric devices using BIT ceramics. In addition, because RUS enables the determination of the temperature dependence of elastic constants, the determination procedure provided in this study paves the way for determination of the temperature dependence of the full matrix constants of BIT ceramics.

Declaration of competing interest

The authors declare that they have no known competing financial interests or personal relationships that could have appeared to influence the work reported in this paper.

Acknowledgments

This work was supported by the National Natural Science Foundation of China (Grant Nos. U2006218, 11674270 and 11874061), State Key Laboratory of Acoustics, Chinese Academy of Science (Grant No. SKLA202108), the Open Research Fund of the Key Laboratory of Sensors, Beijing Information Science and Technology University, and XMU Train Program of Innovation and Entrepreneurship for Undergraduates (Grant Nos. 2019Y1538 and S202010384764).

References

[1] B. Jaffe, W.R. Cook, H. Jaffe, Piezoelectric Ceramics, Academic Press, London, 1971.
[2] K. Nakamura, Ultrasonic Transducers: Materials and Design for Sensors, Actuators and Medical Applications, Woodhead Publishing, Cambridge, 2012.
[3] L.T. Yang, X. Kong, F. Li, H. Hao, Z.X. Cheng, H.X. Liu, J.F. Li, S.J. Zhang, Perovskite lead-free dielectrics for energy storage applications, Prog. Mater. Sci. 102 (2019) 72–108.
[4] H.B. Yang, P.F. Liu, F. Yan, Y. Lin, T. Wang, A novel lead-free ceramic with layered structure for high energy storage applications, J. Alloy, Compd 773 (2019) 244–249.
[5] J.G. Hao, W. Li, J.W. Zhai, H. Chen, Progress in high-strain perovskite piezoelectric ceramics, Math. Sci. Eng. R. 135 (2019) 1–57.
[6] P.K. Panda, Review: environmental friendly lead-free piezoelectric materials, J. Mater. Sci. 44 (19) (2009) 5049–5062.
[7] T. Jardiel, A.C. Caballero, M. Villegas, Aurivillius ceramics: $Bi_4Ti_3O_{12}$-based piezoelectrics, J. Ceram. Soc. Jpn. 116 (1352) (2008) 511–518.
[8] M. Daichi, M. Kobayashi, High performance ultrasonic transducers made by $LiNbO_3/Bi_4Ti_3O_{12}$, in: 2019 IEEE International Ultrasonics Symposium, 2019, pp. 100–103.
[9] X.C. Xie, T.Z. Wang, Z.Y. Zhou, G.F. Cheng, R.H. Liang, X.L. Dong, Enhanced piezoelectric properties and temperature stability of $Bi_4Ti_3O_{12}$-based aurivillius ceramics via W/Nb substitution, J. Eur. Ceram. Soc. 39 (4) (2019) 957–962.
[10] J.L. Xu, C.F.G. Batista, B.R. Tittmann, Practical ultrasonic transducers for high-temperature applications using bismuth titanate and ceramabind 830, in: D. E. Chimenti, L.J. Bond (Eds.), 44th Annual Review of Progress in Quantitative Nondestructive Evaluation, vol. 37, AIP, 2018. Article Number: 100004.
[11] A. Megriche, L. Lebrun, M. Troccaz, Materials of $Bi_4Ti_3O_{12}$ type for high temperature acoustic piezo-sensors, Sensor. Actuat. A–Phys. 78 (2–3) (1999) 88–91.
[12] Y. Kitanaka, Y. Noguchi, M. Miyayama, Y. Kagawa, Elastic and piezoelectric properties of high-quality ferroelectric $Bi_4Ti_3O_{12}$ single crystals, Jpn. J. Appl. Phys. 51 (9) (2012), 09LD08.
[13] H.S. Shulman, M. Testorf, D. Damjanovic, N. Setter, Microstructure, electrical conductivity, and piezoelectric properties of bismuth titanate, J. Am. Ceram. Soc. 79 (12) (1996) 3124–3128.
[14] L. Kozielski, M. Plonska, T. Sebastian, F. Clemens, Dielectric relaxation of $Bi_4Ti_3O_{12}$ ceramics prepared by the low-temperature combustion synthesis, Phase Transitions 91 (9–10) (2018) 1081–1091.
[15] H. Nagata, T. Tokutsu, D. Nakai, Y. Hiruma, T. Takenaka, High temperature piezoelectric properties of vanadium doped $Bi_4Ti_3O_{12}$ ceramics with grain orientation, Ferroelectrics 368 (2008) 440–446.
[16] H. Nagata, S. Matsuzawa, T. Tokutsu, S. Inai, M. Suzuki, Y. Hiruma, T. Takenaka, Temperature dependence of piezoelectric properties on Nd and V co-substituted $Bi_4Ti_3O_{12}$ ceramics for ceramic resonator applications, Ceram. Int. 35 (1) (2009) 163–167.
[17] M. Villegas, A.C. Caballero, T. Jardiel, C. Aragó, J. Maudes, I. Caro, Evaluation of piezoelectric properties of $Bi_4Ti_3O_{12}$-based ceramics at high temperature, Ferroelectrics 393 (1) (2009) 44–53.
[18] A. Safari, E.K. Akdogan, Piezoelectric and Acoustic Materials for Transducer Applications, Springer, New York, 2008.
[19] B.D. Stojanović, C.O. Paiva-Santos, M. Cilense, Č. Jovalekić, Z.Ž. Lazarević, Structure study of $Bi_4Ti_3O_{12}$ produced via mechanochemically assisted synthesis, Mater. Res. Bull. 43 (7) (2008) 1743–1753.
[20] S.E. Cummins, L.E. Cross, Electrical and Optical properties of ferroelectric $Bi_4Ti_3O_{12}$ single crystals, J. Appl. Phys. 39 (5) (1968) 2268–2274.
[21] S.E. Cummins, L.E. Cross, Crystal symmetry, Optical properties and ferroelectric polarization of $Bi_4Ti_3O_{12}$ single crystals, Appl. Phys. Lett. 10 (1) (1967) 14–16.
[22] Z.H. Peng, Q. Chen, Y. Chen, D.Q. Xiao, J.G. Zhu, Microstructure and electrical properties in W/Nb co-doped aurivillius phase $Bi_4Ti_3O_{12}$ piezoelectric ceramics, Mater. Res. Bull. 59 (2014) 125–130.
[23] E.K. Choi, S.S. Kim, J.K. Kim, J.C. Bae, W.J. Kim, Y.I. Lee, T.K. Song, Effects of donor ion doping on the orientation and ferroelectric properties of bismuth titanate thin films, Jpn. J. Appl. Phys. 43 (1) (2004) 237–241.
[24] ANSI IEEE Standard on Piezoelectricity, Std 176-1987, IEEE Standards Association, New York, 1987.
[25] V.Y. Topolov, Comment on "Complete sets of elastic, dielectric, and piezoelectric properties of flux-grown [011]-poled $Pb(Mg_{1/3}Nb_{2/3})O_3$-(28-32)%$PbTiO_3$ single crystals, [Appl. Phys. Lett. 92 (2008) 142906. Appl. Phys. Lett. 92(19) (2010) 196101.
[26] V.Y. Topolov, C.R. Bowen, Inconsistencies of the complete sets of electromechanical constants of relaxor-ferroelectric single crystals, J. Appl. Phys. 109 (9) (2011), 094107.
[27] L.G. Tang, W.W. Cao, Temperature dependence of self-consistent full matrix material constants of lead zirconate titanate ceramics, Appl. Phys. Lett. 106 (5) (2015), 052902.
[28] R.G. Leisure, F.A. Willis, Resonant ultrasound spectroscopy, J. Phys. Condens. Mat. 9 (28) (1997) 6001–6029.
[29] R.B. Schwarz, J.F. Vuorinen, Resonant ultrasound spectroscopy: applications, current status and limitations, J. Alloy, Compd 310 (2000) 243–250.
[30] A. Migliori, J.L. Sarrao, W.M. Visscher, T.M. Bell, M. Lei, Z. Fisk, R.G. Leisure, Resonant ultrasound spectroscopic techniques for measurement of the elastic moduli of solids, Physica B 183 (1–2) (1993) 1–24.
[31] I. Ohno, Rectangular parallellepiped resonance method for piezoelectric crystals and elastic constants of alpha-quartz, Phys. Chem. Miner. 17 (5) (1990) 371–378.
[32] H. Ogi, Y. Kawasaki, M. Hirao, H. Ledbetter, Acoustic spectroscopy of lithium niobate: elastic and piezoelectric coefficients, J. Appl. Phys. 92 (5) (2002) 2451–2456.
[33] H. Ogi, T. Ohmori, N. Nakamura, M. Hirao, Elastic, anelastic, and piezoelectric coefficients of alpha-quartz determined by resonance ultrasound spectroscopy, J. Appl. Phys. 100 (5) (2006), 053511.
[34] N. Nakamura, H. Ogi, M. Hirao, Elastic, anelastic, and piezoelectric coefficients of GaN, J. Appl. Phys. 111 (1) (2012), 013509.
[35] C.W. Chen, S.X. Liu, X. Tan, L.G. Tang, W.W. Cao, Accurate characterization of complete set constants of single domain 0.72$Pb(Mg_{1/3}Nb_{2/3})O_3$-0.28$PbTiO_3$ single crystal by resonant ultrasound spectroscopy using only one sample, J. Appl. Phys. 125 (6) (2019), 064102.
[36] Y. Xiang, C.W. Chen, L.G. Tang, L. Qin, H.M. Zhu, W.W. Cao, Dielectric, elastic and piezoelectric properties of single domain $Pb(Zn_{1/3}Nb_{2/3})O_3$-6.5%$PbTiO_3$ single crystal with 3m symmetry measured using one sample, Scripta Mater. 194 (2021) 113634.
[37] J. Pujol, The solution of nonlinear inverse problems and the Levenberg-Marquardt method, Geophys 72 (4) (2007) W1–W16.
[38] M. Landa, P. Sedlák, H. Seiner, L. Heller, L. Bicanová, P. Šittner, V. Novák, Modal resonant ultrasound spectroscopy for ferroelastics, Appl. Phys. A–Mater. 96 (3) (2009) 557–567.
[39] D.H. Hurley, S.J. Reese, F. Farzbod, Application of laser-based resonant ultrasound spectroscopy to study texture in copper, J. Appl. Phys. 111 (5) (2012), 053527.
[40] F. Farzbod, O.E. Scott-Emuakpor, Resonant ultrasound spectroscopy: sensitivity analysis for isotropic materials and anisotropic materials with cubic symmetry, J. Vib. Acoust. 141 (2) (2019), 021010.
[41] P. Sedlák, H. Seiner, J. Zídek, M. Janovská, M. Landa, Determination of all 21 independent elastic coefficients of generally anisotropic solids by resonant ultrasound spectroscopy: benchmark examples, Exp. Mech. 54 (6) (2014) 1073–1085.